Supplementary information

for

Antiferromagnetic ordering and signatures of enhanced spin-frustration in honeycomb-layered tellurates with Ag bilayers

Sachio Komori[1]*, Kohei Tada[2]*, Noboru Taguchi[2], Tomoyasu Taniyama[1], Titus Masese[2]*

[1]Department of Physics, Nagoya University, Furo-cho, Chikusa-ku, Nagoya 464-8602, Japan

[2]Research Institute of Electrochemical Energy, National Institute of Advanced Industrial Science and Technology, 1-8-31 Midorigaoka, Ikeda, Osaka 563-8577, Japan

* komori.sachio.h0@f.mail.nagoya-u.ac.jp *k-tada@aist.go.jp *titus.masese@aist.go.jp

1. Interslab exchange coupling in honeycomb-layered tellurates

To investigate an interslab magnetic exchange coupling of (Te, *M*)-O magnetic layers through a cationic layer (denoted X layer), we have calculated the total energy difference between layered-antiferromagnetic (L-AFM) and ferromagnetic (FM) ordering [$\Delta E = E(\mathrm{FM}) - E(\text{L-AFM})$] for various X layers, which are plotted in Fig. S1 (left-axis). Larger ΔE indicates larger interslab exchange coupling (the L-AFM state is more stable than the corresponding FM state due to the exchange coupling). ΔE exponentially decreases with increasing thickness of the X layer (right-axis of Fig. S1). Although the ionic radius of Ag^+ is comparable to Na^+, a dumbbell like straight coordination through the *d*-orbital of Ag^+ results in a large interslab distance and a stronger suppression of the interslab magnetic exchange coupling in $Ag_{2-x}M_2TeO_6$ ($0 < x < 2$) than that in $Na_2M_2TeO_6$. Moreover, the interslab distance of $Ag_6M_2TeO_6$ is even longer (9 Å[26]) than that of $Ag_{2-x}M_2TeO_6$ (6 Å[26]), implying a further suppression of the magnetic exchange coupling due to the presence of Ag bilayers.

The exchange-correlation functional used for the density functional theory (DFT) calculation was the generalised gradient approximation formula of Perdew-Burke-Ernzerhof (GGA-PBE) [1], and the basis set was plane-wave with projector-augmented-wavefunction (PAW) method [2]. The electrons in the inner core regions were treated by PAW, and the numbers of valence electrons of Li, Na, K, Rb, Ag, Ni, Te, and O were 1 ($2s^1$), 1 ($3s^1$), 7 ($3p^6 4s^1$), 7 ($4p^6 5s^1$), 11 ($4d^{10} 5s^1$), 10 ($3d^8 4s^2$), 6 ($5s^2 5p^4$) and 6 ($2s^2 2p^4$), respectively. The energy cut-offs for wavefunction and augmented charge were 500 eV and 2400 eV. To correct repulsions among the 3*d* electrons of Ni, DFT+*U* method was used (the applied *U* value was 4.0 eV) [3]. Dispersion forces were corrected by DFT-D3 scheme using the parameter with

Becke-Jonson damping [4]. The sampled *k*-points were on the Γ-centred mesh of 5×5×3. The DFT calculations were performed by VASP programme [5].

Due to the non-subtleties of pseudo-spin simulation using Kohn-Sham formalism in VASP, we considered the simulation of the recently predicted Ag degenerate states in Ag bilayers[26] as beyond our present scope. Even if a pseudo-spin moment of Ag bilayered structures presents, the small moment is unlikely to affect the interslab exchange coupling and therefore the Ag-bilayered $Ag_6Mg_2TeO_6$ should also follow the trend in Fig. S1.

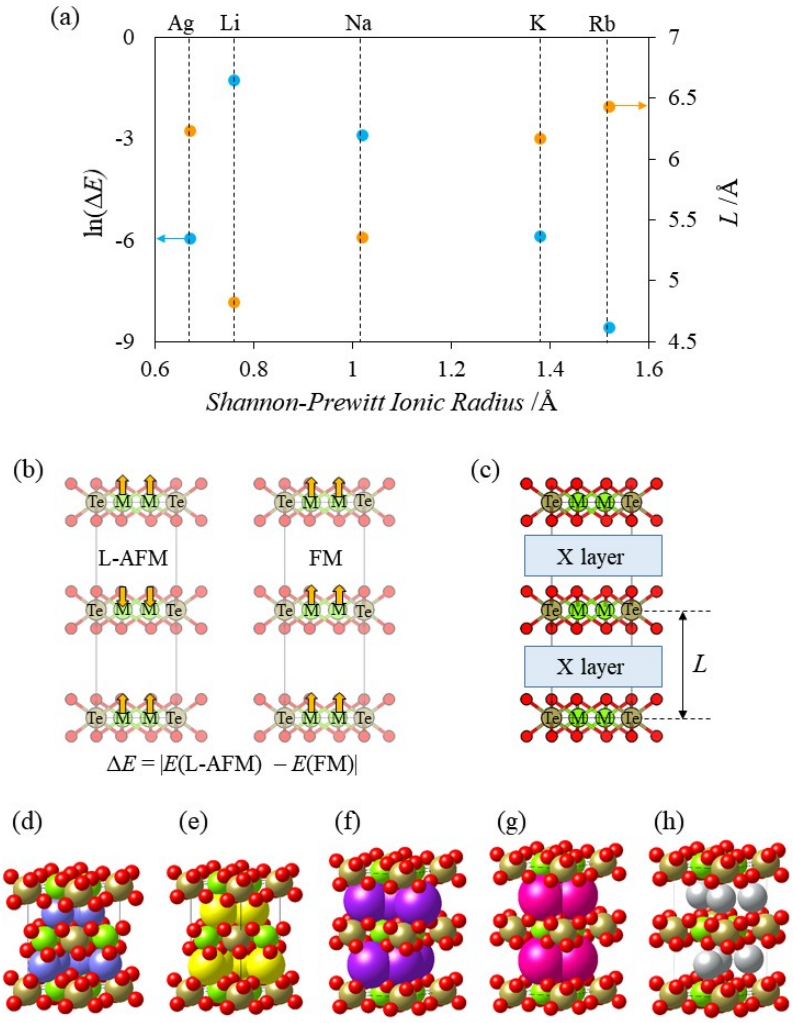

Fig. S1 (a) Difference of the total energy between FM and layered (L)-AFM states (left-axis) and interslab distance (right-axis) for mono-layered $X_2M_2TeO_6$ with a single cationic X layer (X = Li, Na, K, Rb, and Ag). (b) Schematic views of L-AFM and FM spin configurations. (c) Schematic view of (Te, *M*)-O magnetic layers separated by a distance *L*. Crystal structures of $X_2M_2TeO_6$ with X = (d) Li, (e) Na, (f) K, (g) Rb, and (h) Ag.

2. Magnetic properties of $Ag_2Mg_2TeO_6$

To investigate the presence of pseudo-spins in the Ag-bilayers, we measured magnetic properties of $Ag_2Mg_2TeO_6$ (M = Mg) which does not have magnetic honeycomb slabs and therefore suitable to detect the moment from the pseudo-spins. Figure S2(a) shows the magnetic susceptibility (χ) versus temperature (T) curve at the magnetic field (H) of 100 Oe. χ at 300 K is about 3 orders of magnitude smaller than that of M = Co, $Co_{0.5}Ni_{0.5}$, and Ni [Figs. 2(a)-(c) in the main paper]. Although an increase of χ with decreasing T is observed, the T-dependence deviates from the Curie-Weiss law, suggesting that a paramagnetic moment is not predominant in M = Mg, which is in sharp contrast to M = Co, CoNi, and Ni. From moment versus field [$m(H)$] curve at 10 K [Fig. S2(b)], we identify a small fraction of ferromagnetic ordering with the saturation moment and field of about 0.1 emu mol^{-1} and 1 kOe, respectively. The ferromagnetic ordering is also observable in M = Co, $Co_{0.5}Ni_{0.5}$, and Ni, which manifests as a peak near zero field in their dm/dH curve as shown in Fig. S2(c). However, further study is necessary to clarify the relation between the ferromagnetic order and the pseudo-spins in the Ag bilayers.

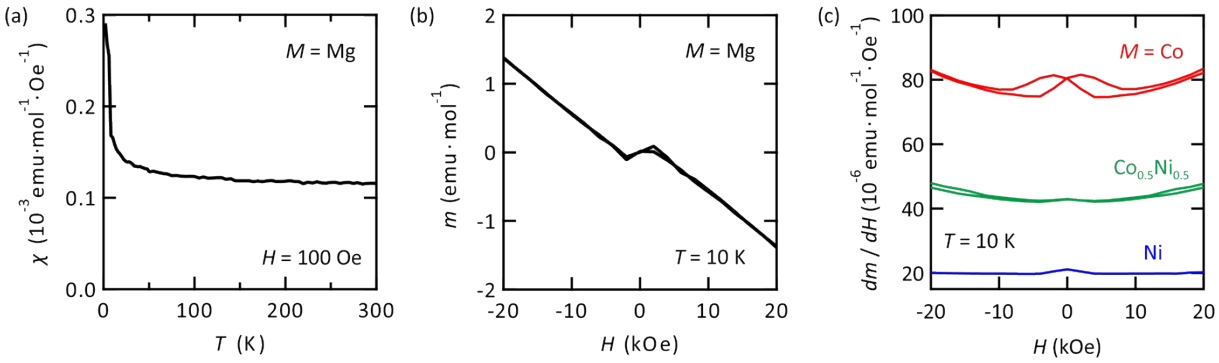

Fig. S2 (a) χ versus T at H = 100 Oe measured during cooling and (b) m versus H at T = 10 K for $Ag_2Mg_2TeO_6$ (M = Mg) polycrystalline powders. (c) dm/dH versus H for at T = 10 K for M = Co (the red curve), $Co_{0.5}Ni_{0.5}$ (the green curve), and Ni (the blue curve).

3. Estimation of the spin-flop transition field

In Fig. S3(a), we plot the temperature dependence of the $m(H)$ curve for M = $Co_{0.5}Ni_{0.5}$. At low temperatures (4 K and 20 K) below the Néel temperature (T_N), the $m(H)$ curve is non-linear, indicating the presence of a broad spin-flop transition. Figure S3(b) shows the $m(H)$ and dm/dH (H) curves at 10 K for M = $Co_{0.5}Ni_{0.5}$. We have estimated the transition field from the field giving the maximum of dm/dH

[6] (H = 60 kOe). We note that the transition can occur in a broad field range around H = 60 kOe due to factors such as a size variation of the polycrystalline powder sample.

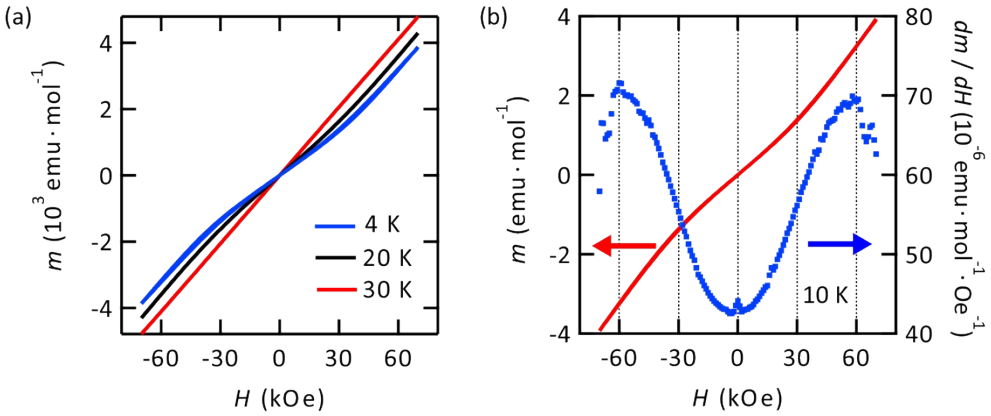

Fig. S3 (a) m versus H at T = 4 (the blue curve), 20 (the black curve), 30 K (the red curve) for M = $Co_{0.5}Ni_{0.5}$. (b) m (the red curve; left-axis) and dm/dH (the blue dots; right-axis) versus H at T = 10 K for M = $Co_{0.5}Ni_{0.5}$.

[1] Perdew, J. P., Burke, K. & Ernzerhof, M. Generalized Gradient Approximation Made Simple. Phys. Rev. Lett. 77, 3865 (1996).

[2] Kresse, G., and Joubert, D, From ultrasoft pseudopotentials to the projector augmented-wave method. Phys. Rev. B 59, 1758 (1999).

[3] Blöchl, P. E., Projector augmented-wave method, Phys. Rev. B, 50, 17953 (1994); Dudarev, S. L. et al. Electron-energy-loss spectra and the structural stability of nickel oxide: An LSDA+U study. Phys. Rev. B 57, 1505 (1998).

[4] Grimme, S., Antony, J., Ehrlich, S. & Krieg, H. A consistent and accurate ab initio parametrization of density functional dispersion correction (DFT-D) for the 94 elements H-Pu. J. Chem. Phys. 132, 154104 (2010); Grimme, S., Ehrlich, S. & Goerigk, L. Effect of the damping function in dispersion corrected density functional theory. J. Comput. Chem. 32, 1456 (2011).

[5] Kresse, G., and Hafner, J. Ab initio molecular dynamics for liquid metals. Phys. Rev. B 47, 558 (1993); Kresse, G., and Hafner, J. Ab initio molecular-dynamics simulation of the liquid-metal–amorphous-semiconductor transition in germanium. Phys. Rev. B 49, 14251 (1994); Kresse, G., and Furthmüller, J. Efficient iterative schemes for ab initio total-energy calculations using a plane-wave basis set. Phys.

Rev. B 54, 11169 (1996); Kresse, G. and Furthmüller, J. Efficiency of ab-initio total energy calculations for metals and semiconductors using a plane-wave basis set. Comput. Mater. Sci. 6, 15–50 (1996).

[6] Viciu, L., Huang, Q., Morosan, E., Zandbergen, H. W., Greenbaum, N. I., McQueen, T., and Cava, R. J., Structure and basic magnetic properties of the honeycomb lattice compounds $Na_2Co_2TeO_6$ and $Na_3Co_2SbO_6$. J. Solid State Chem. 180, 1060–1067 (2007).